Multi-Wavelength Imaging of Young Stellar Object Disks: Toward an Understanding of Disk Structure and Dust Evolution

Alan M. Watson
Universidad Nacional Autónoma de México

Karl R. Stapelfeldt
Jet Propulsion Laboratory, California Institute of Technology

Kenneth Wood
University of St. Andrews

François Ménard
Laboratoire d'Astrophysique de Grenoble

We review recent progress in high-resolution imaging of scattered light from disks around young stellar objects. Many new disks have been discovered or imaged in scattered light, and improved instrumentation and observing techniques have led to better disk images at optical, near-infrared, and thermal-infrared wavelengths. Multi-wavelength datasets are particularly valuable, as dust particle properties have wavelength dependencies. Modeling the changes in scattered-light images with wavelength gives direct information on the dust properties. This has now been done for several different disks. The results indicate that modest grain growth has taken place in some of these systems. Scattered-light images also provide useful constraints on the disk structure, especially when combined with long-wavelength SEDs. There are tentative suggestions in some disks that the dust may have begun to settle. The next few years should see this work extended to many more disks; this will clarify our understanding of the evolution of protoplanetary dust and disks.

1. INTRODUCTION

This chapter reviews the progress since the *Protostars and Planets IV* meeting (*McCaughrean et al.*, 2000) in observations and modeling of scattered-light images of disks around young stellar objects (YSOs). For many years these disks were studied in the infrared and at millimeter wavelengths, but without the spatial resolution necessary to reveal their detailed structure. With the advent of the *Hubble Space Telescope* (HST) and ground-based adaptive optics (AO) systems, these disks were seen in scattered optical and near-infrared starlight. The first images of disks in scattered light showed them as never before. These images currently provide the highest spatial resolution images of disks and provide unique information on disk structure and dust properties.

Most disks around young low- and intermediate-mass stars fall into one of two categories on the basis of their gross observational properties. YSO disks are optically thick at visible and near-infrared wavelengths, are rich in molecular gas, and are found around Class I and Class II systems. Debris disks are optically thin at optical and near-infrared wavelengths, have only trace quantities of gas, and are found around Class III and older systems.

Our current understanding of the evolution of dust in disks around young low- and intermediate-mass stars is that these observational categories correspond to very distinct phases. In YSO disks our understanding is that gas and dust from molecular cores is processed through the disk and provides the raw material both for accretion and outflows. The dust is processed first in the dense molecular core and then in the disk itself. The dust grows and suffers chemical processing. Dust growth is hypothesized to result in the production of planetesimals, which form rocky planets and the cores of gas giant planets. In debris disks, our understanding is that dust is present largely as a result of collisions between planetesimals. Thus, YSO disks are thought to be characterized by dust growth whereas debris disks are thought to characterized by planetesimal destruction.

In this chapter we focus on observations and modeling of scattered-light images of YSO disks around low- and intermediate-mass stars. That is, we focus on the phase in which dust is expected to grow. Of course, scattered-light observations and models are not the only means to explore these disks. The chapter by *Dutrey et al.* discusses millimeter and sub-millimeter observations of the gas and dust components and the chapters by *Bouvier et al.*, *Najita et al.*, *Millan-Gabet et al.* cover observations of the inner disk region, notably interferometry, and their interpretations. The

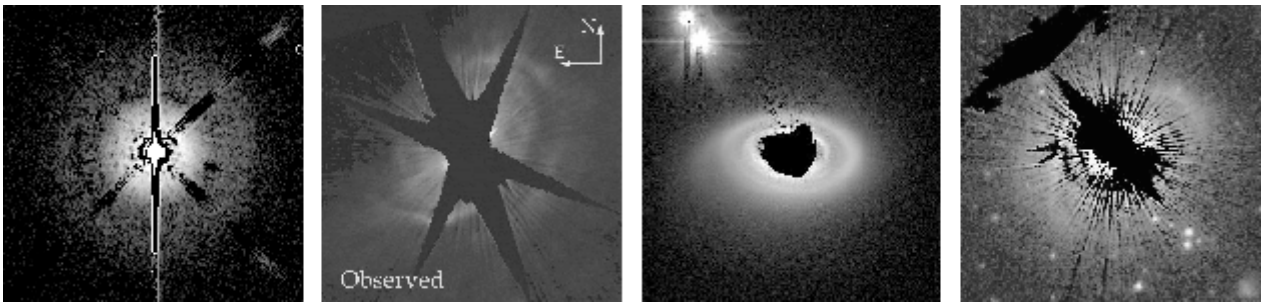

Fig. 1.— Scattered light images of four face-on or intermediate inclination YSO disks newly resolved since 1998. Left-to-right: TW Hya face-on disk (*Krist et al.*, 2000), HD 100546 (*Grady et al.*, 2001), HD 141569A (*Clampin et al.*, 2003), and HD 163296 (*Grady et al.*, 2000).

chapter by *Monin et al.* discusses aspects of disks that are peculiar to binaries. Further from the subject of our chapter, the chapter by *Cesaroni et al.* discusses disks around young high-mass stars and the chapter by *Meyer et al.* reviews debris disks around solar-type stars.

In the following sections we summarize the data available on scattered-light disks around YSOs, imaging techniques, and what we can learn about disk structure and dust properties from modeling multi-wavelength images and SEDs. We also speculate about future advances.

2. OBSERVATIONAL PROGRESS

At the time of the *Protostars and Planets IV* meeting, held in 1998, only a dozen YSO disks had been resolved in scattered light and another half dozen in silhouette against the Orion nebula. Since then, the number of resolved disks in these two categories has doubled and quadrupled, respectively. The new discoveries stem largely from targeted high-contrast imaging of greater numbers of YSOs and wide-field imaging surveys of star-forming clouds. In the optical and near-infrared, the broader application of established observing techniques, rather than any instrumental improvements, has driven the recent expansion in the number of disks discovered. At longer mid-infrared wavelengths, larger telescopes equipped with more potent mid-infrared imagers became available. These results are described in this section and images of some of the new disks are shown in Figs. 1 and 2. A complete list of published YSO disks resolved in scattered light appears in Table 1. Most of these are around T Tau stars, although some are around Herbig AeBe stars. An on-line catalog of circumstellar disks resolved in scattered light, thermal emission, or molecular lines is now available; the URL is http://www.circumstellardisks.org.

2.1. Optical and Near-Infrared Imaging

2.1.1 Coronagraphic and Direct Imaging. The most general case, and also the most observationally challenging, is the detection of disk scattered light in the presence of direct starlight. Subtraction of a fiducial reference star is almost always necessary to reveal the disk, and a coronagraph is usually employed to suppress stellar diffraction. Various HST instruments have produced excellent images of disks around bright stars, while groundbased AO imaging of these disks is often hampered by the instability of the point spread function.

The brightness of Herbig AeBe stars makes them excellent disk imaging targets, and three have been found to show interesting circumstellar nebulosity. HD 100546 has a disk viewed from high latitudes which contains what appear to be two spiral arms (*Pantin, Waelkens, and Lagage*, 2000; *Grady et al.*, 2001; *Augereau et al.*, 2001). HD 163296 shows an inclined disk with a hint of a cleared central zone and bifurcation into upper and lower reflection nebulosities (*Grady et al.*, 2000). The nebulosity around AB Aur shows a wealth of structure (*Grady et al.*, 1999; *Fukagawa et al.*, 2004), but it is unclear how much is associated with the disk and how much with a more extended envelope. *Fukagawa et al.* (2003) report a possible disk around HD 150193A.

The transitional disk HD 141569A has been the subject of a great deal of observational and theoretical work. The first images in the near-infrared by *Weinberger et al.* (1999) and *Augereau et al.* (1999) appeared to show a large radial clearing in the disk at a radius of 250 AU. Optical imaging by *Mouillet et al.* (2001) and *Clampin et al.* (2003) revealed an asymmetric spiral-like feature and showed that the cleared region was not completely empty. HD 141569A is in a multiple system. Dynamical studies suggest that stellar fly-bys or a recent periastron passage by the companions could be the origin of the observed spiral feature (*Augereau and Papaloizou*, 2004; *Ardila et al.*, 2005; *Quillen et al.*, 2005).

Perhaps the most significant new disk imaged around a directly visible star since *Protostars and Planets IV* is that of TW Hya (*Krist et al.*, 2000; *Trilling et al.*, 2001; *Weinberger et al.*, 2002). This face-on disk is also the closest T Tauri star disk, at a distance of 56 pc, and has been well-studied at millimeter wavelengths. The disk radial profile shows a sharp break in slope at a radius of 140 AU which is seen in multiple independent datasets. The physical origin of this sudden fading in the outer disk is unclear. Long-slit spectra of the TW Hya disk with HST STIS (*Roberge et al.*, 2005) find that the disk has a roughly neutral color from 5000 Å to 8000 Å (see their Fig. 5), consistent with previ-

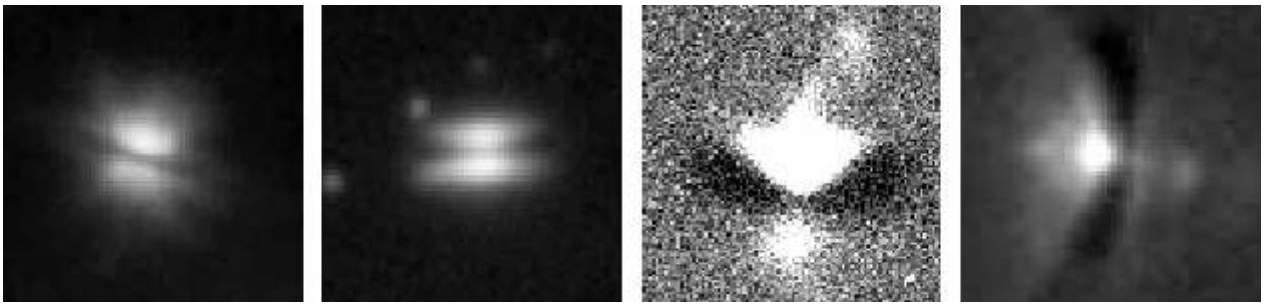

Fig. 2.— Scattered light images of four edge-on or silhouette YSO disks newly resolved since 1998. Left-to-right: Edge-on disks of HV Tau C (*Stapelfeldt et al.*, 2003), 2MASSI1628137-243139 (*Grosso et al.*, 2003), IRAS 04158+2805 (*Ménard et al.*, in preparation), and Orion 216-0939 (*Smith et al.*, 2005).

ous broad-band imaging in the same spectral region (*Krist et al.*, 2000) and near-infrared (*Weinberger et al.*, 2002).

Despite the interesting results highlighted above, most YSO disks (those whose presence is inferred from infrared and submm excess emission) remain undetectable in scattered light. There are probably multiple reasons for this fact. Disks with outer radii smaller than $0.5''$, the typical inner working angle cutoff for current coronagraphs and PSF subtraction techniques, would not extend far enough from their host star to be readily detected. This cannot be the whole explanation, however; the disk of MWC 480 has a large outer radius in millimeterwave CO emission (*Simon et al.*, 2000), but repeated attempts to detect it in scattered light have failed (*Augereau et al.*, 2001; *Grady et al.*, 2005). There are other examples. Many disks may simply be intrinsically fainter than the ones that have been imaged in scattered light to date; they may be geometrically flatter (and thus tending toward self-shadowing), depleted of small particles, or have undergone chemical processing that has reduced their albedo. With the typical YSO disk currently undetectable against the direct light of its parent star, improved coronagraphic instrumentation will be needed to understand the diversity in disk scattering properties and their underlying causes.

2.1.2 Edge-On Disks. Edge-on, optically thick disks naturally occult their central stars and in the process present their vertical structure to direct view. Observations of edge-on disks require high spatial resolution but not high contrast, so AO systems are competitive. Furthermore, the absence of stellar PSF artifacts make edge-on systems particularly amenable to scattered light modeling. Two of the first known examples, HH 30 and HK Tau B, have been extensively studied over the past few years, and are discussed at greater length in sections 2.4, 5.1, and 5.2 below. Additional examples are very valuable for comparative studies of disk scale heights, flaring, and dust properties. Finding new edge-on disks and imaging them across a wide range of wavelengths are high priorities for future research.

The edge-on disk CRBR 2422.8 was discovered in the ρ Oph cloud core by *Brandner et al.* (2000a). A model for the source combining scattered light images and mid-infrared spectra is presented by *Pontoppidan et al.* (2005). Near ρ Oph lies another new edge-on disk, 2MASSI1628137-243139. *Grosso et al.* (2003) discovered and present models for this object and note a peculiar near-IR color difference between the two lobes of its reflection nebula. Three new edge-on disks have been found via adaptive optics as companions to brighter stars. *Jayawardhana et al.* (2002) and *Chauvin et al.* (2002) discovered LkHα 263C in a quadruple system, and *Jayawardhana et al.* present initial models suggesting a disk mass of 0.002 $M_{\odot}$. PDS 144 is a compact edge-on disk around a companion to an Ae star (*Perrin et al.*, in preparation). The mysterious nature of HV Tau C was finally resolved by *Monin and Bouvier* (2000) to be an edge-on disk around the tertiary star. Modeling of HST images of HV Tau C by *Stapelfeldt et al.* (2003) indicates that this disk also possesses a small circumstellar envelope. Finally, a new kind of edge-on disk has been identified around the Perseus source ASR 41: an extended shadow from a (presumably) compact disk is cast across foreground cloud material (*Hodapp et al.*, 2004).

2.1.3 Silhouette Disks. The Orion Nebula continues to be a unique and fertile ground for finding new resolved disks. Several hundred compact ionized globules ("proplyds") likely contain circumstellar disks, but have a morphology dominated by photoevaporative processing in their H II region environment. Some of these contain internal silhouettes clearly reminiscent of disks; and there is also a distinct category of pure silhouette disks lacking any external ionization. In both cases, the disk silhouettes are visible in Hα images as foreground absorption to the H II region. New silhouette sources are reported in a comprehensive paper by *Bally et al.* (2000), and by *Smith et al.* (2005). A particularly interesting new source is Orion 216-0939; like Orion 114-426 (*McCaughrean et al.*, 1998; *Shuping et al.*, 2003), this is a giant edge-on silhoutte more than 1000 AU in diameter, and with bipolar reflection nebulae.

Despite the discovery of proplyds in M8 (*Stecklum et al.*, 1998) and NGC 3603 (*Brandner et al.*, 2000b) and despite HST imaging of NGC 2024, NGC 2264, M16, M17, and Carinae, no silhouette disks have been identified in H II regions other than Orion. *Ménard et al.* (in preparation) found the first example of a silhouette disk in nearby Taurus clouds: IRAS 04158+2805 shows a cone of scattered

TABLE 1
YSO DISKS IMAGED IN SCATTERED LIGHT

Object Name	Type	Outer Radius	Recent Reference
TW Hya	face-on	220 AU	*Roberge et al.* (2005)
HD 141569	transition	370 AU	*Clampin et al.* (2003)
HD 100546	spiral	360 AU	*Grady et al.* (2005)
HD 163296		450 AU	*Grady et al.* (2005)
HD 150193A		190 AU	*Fukagawa et al.* (2003)
AB Aur	disk+envelope	$>$ 300 AU	*Fukagawa et al.* (2004)
CB 26	edge-on	380 AU	*Stecklum et al.* (2004)
CRBR 2422.8-3423	edge-on	105 AU	*Pontoppidan et al.* (2005)
DG Tau B	edge-on	270 AU	*Padgett et al.* (1999)
GG Tau	CB ring	260 AU	*Krist et al.* (2005)
GM Aur		500 AU	*Schneider et al.* (2003)
HH 30	edge-on	225 AU	*Watson & Stapelfeldt* (2004)
HK Tau B	edge-on	105 AU	*McCabe et al.* (2003)
HV Tau C	edge-on	85 AU	*Stapelfeldt et al.* (2003)
Haro 6-5B	edge-on	280 AU	*Padgett et al.* (1999)
IRAS 04302+2247	edge-on	420 AU	*Wolf et al.* (2003)
UY Aurigae	CB ring	2100 AU	*Potter et al.* (2000)
2MASSI J1628137-243139	edge-on	300 AU	*Grosso et al.* (2003)
IRAS 04325+2402	edge-on	30 AU	*Hartmann et al.* (1999)
OphE-MM3	edge-on	105 AU	*Brandner et al.* (2000a)
ASR 41	shadow	$<$ 3100 AU	*Hodapp et al.* (2004)
LkHα 263 C	edge-on	150 AU	*Jayawardhana et al.* (2002)
Orion 114-426	edge-on	620 AU	*Shuping et al.* (2003)
Orion 216-0939	edge-on	600 AU	*Smith et al.* (2005)

light, a jet, and a silhouette 3000 AU in diameter projected in front of diffuse Hα emission near V892 Tau.

2.2. Mid-Infrared Imaging

The usual objective when imaging YSOs in the mid-infrared is to resolve extended thermal emission from their inner disks. At the distances of the nearest star-forming clouds, extended 10–20 μm thermal emission has only been detected in a handful of luminous Ae stars (HD 100546, AB Aur, and V892 Tau; *Liu et al.*, 2003, 2005; *Chen and Jura*, 2003; *Pantin et al.*, 2005). In lower-luminosity T Tauri stars, the 10–20 μm emssion is spatially unresolved – even in the relatively nearby case of TW Hya (*Weinberger et al.*, 2002). The absence of extended 20 μm emission in T Tauri stars may pose a problem for models of flared disk spectral energy distributions (*Chiang and Goldreich*, 1997). These models postulate a superheated disk upper layer where stellar radiation is predominantly absorbed by small dust particles, which then radiate inefficiently at longer wavelengths. Large grains or flatter disks may be needed to explain the fact that most of these sources are unresolved in the mid-infrared.

One of the more significant and surprising disk imaging results of recent years has been the detection of *scattered light* from three YSO disks in the mid-infrared. *McCabe et al.* (2003) found that the edge-on disk of HK Tau B appears as an extended source in sensitive 10 μm Keck images. The good alignment of this 10 μm nebulosity with the optical scattered light (*Stapelfeldt et al.*, 1998), its extent well beyond a reasonable diameter for disk thermal emission, and its monotonically declining flux density from 2 to 10 μm argue that this is scattered light. It is not clear if the original source of emission is the star or the inner part of the disk. The fact that some edge-on disks might be seen entirely via scattered light in the mid-infrared was already indicated by *Infrared Space Observatory* photometry of HH 30 (*Wood et al.*, 2002); HK Tau B is the first resolved example. A second is in the case of GG Tau, where *Duchêne et al.* (2004) clearly detect the circumbinary ring in deep 3.8 μm images. By the same arguments as above, this must also be scattered light. A third source, PDS 144 (*Perrin et al.*, in preparation), is an A star that appears as a spectacular bipolar nebula in 10 μm images; the relative contributions of scattered light and PAH emission in this image are still being assessed. As discussed in section 5.3 below, scattered light at these long wavelengths is a powerful diagnostic of large grains in circumstellar disks. Additional examples of resolved mid-IR scattered light from YSO disks can be expected in the future.

2.3. Polarimetric Imaging

Imaging polarimetry can confirm the presence of scattered light nebulosity and offer clues to the location of embedded illuminating sources. The strength of the ob-

served polarization depends on the dust grain properties, the scattering geometry, the degree of multiple scattering, and the polarization induced by any foreground cloud material. Spatially resolved polarimetry has been reported for only a few disks. The best example is GG Tau, where the geometry of the circumbinary ring is very well understood, and thus the polarimetric results can be readily interpreted. *Silber et al.* (2000) found that backscattered light from the far side of the ring was very highly polarized at 1 μm, requiring that the scattered light originate from submicron-sized grains.

A new application for polarimetry has emerged in high contrast AO. Groundbased AO systems provide a diffraction-limited image core, but also an extended, uncontrolled seeing halo. The light from this halo can overwhelm the faint nebulosity of a circumstellar disk. Differential polarimetry exploits the fact that scattered light from YSO disks is highly polarized while the seeing halo has virtually zero polarization. By simultaneously imaging in two polarizations, the unpolarized halo can be removed, and the polarized disk light more clearly seen. *Potter* (2003) and *Perrin et al.* (2004) report detections of several YSO nebulosities with this technique; most are circumstellar envelopes. A few disks have also been studied with this technique, notably TW Hya (*Apai et al.*, 2004) and LkCa 15 (*Potter*, 2003). The latter has not been detected in several conventional unpolarized imaging searches.

2.4. Variability

T Tauri stars commonly show photometric variability on timescales of a few days to months. In the youngest stars, these variations are now thought to be the result of hot spots, variation in accretion rate, and occultation by warps in the inner disk, all of which are natural consequences of magnetospheric accretion mechanism discussed in the chapter by *Bouvier et al.* Disks also show variability, and in this section we describe the best studied cases, HH 30 and AA Tau.

2.4.1 Photometric Variability in HH 30. Similarly to their central stars, disks show photometric variability. The scattered light from the disk should follow as the star brightens and fades. The integrated magnitude of HH 30 varies on timescales of a few days over a range of more than one magnitude in both V and I (*Wood et al.*, 2000). The range is slightly greater in V than in I. Early photometry suggested that the variability was periodic, but subsequent studies have not confirmed this.

The range of variability of the disk is likely to be a lower limit on the range of variability of the star, as the multiple optical paths taken by scattered light will likely act to smooth the stellar variations to some degree, both because of the finite speed of light (173 AU per day) and because the disk is illuminated by light from a range of stellar azimuths. Cool spots produce stellar variability with ranges of no more than one magnitude (*Herbst et al.*, 1994), and so cannot explain the variability of the disk. Some other mechanism must be at work in HH 30, perhaps hot spots, variations in accretion rate, or occultations. This is consistent with the strong veiling component observed by *White and Hillenbrand* (2004).

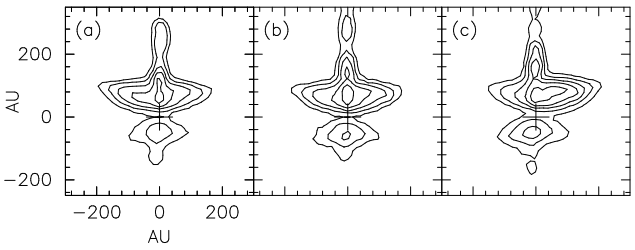

Fig. 3.— HST/WFPC2 images showing the morphological variability of HH 30 (*Watson and Stapelfeldt*, in preparation). The images are from (a) 2001 February, (b) 1995 January, and (c) 1998 March. All images were taken in a broad filter centered at 675 nm. The images show the left side brighter, both sides having similar brighnesses, and the right side brighter.

2.4.2 Morphological Variability in HH 30. More interesting and unexpected are the quantitative changes in the morphology of the scattered light (*Burrows et al.*, 1996; *Stapelfeldt et al.*, 1999; *Cotera et al.*, 2001; *Watson and Stapelfeldt*, in preparation). These include changes in the contrast between the brighter and fainter nebulae over a range of more than one magnitude; changes in the lateral contrast between the two sides of the brighter nebula over a range of more than one magnitude (see Fig. 3); and changes in the lateral contrast between the two sides of the fainter nebula over a range of about half a magnitude.

The timescales for the variability are uncertain, but are less than one year. Thus, the variability is not due to changes in the disk structure at radii of 100 AU but rather changes in the pattern of illumination at radii of 1 AU or less. Thus, this *morphological* variability is fascinating as it allows us to peek into the central part of the disk and possibly constrain the geometry of the accretion region.

However, before we use the variability to constrain anything, we need to understand its origin. Two mechanisms have been suggested; *Wood and Whitney* (1998) have suggested that inclined hot spots could illuminate the outer parts of disk like lighthouses, and *Stapelfeldt et al.* (1999) have suggested that warps in the inner disk could cast shadows over the outer disk.

In the case of HH 30, one might hope to distinguish between the mechanisms on the basis of the color of the morphological variability. HST observations show no significant differences between V and I. Naively, one would expect illumination by hot spots to produce stronger variability in the blue whereas optically-thick shadowing should be neutral in color. However, spectroscopic studies show that the veiling component is often relatively flat in the red (*Basri and Batalha*, 1990; *White and Hillenbrand*, 2004), so the lack of color is inconclusive.

Determining the timescale might help to distinguish between the mechanisms, although if the putative warp in the inner disk is locked to the star as it appears to be in AA

TABLE 2
PUBLICLY AVAILABLE SCATTERING AND THERMAL EQUILIBRIUM CODES

Code	URL
HO-CHUNK	http://gemelli.colorado.edu/~bwhitney/codes/codes.html
MC3D	http://www.mpia-hd.mpg.de/FRINGE/SOFTWARE/mc3d/mc3d.html
Pinball	http://www.astrosmo.unam.mx/~a.watson/
RADMC and RADICAL	http://www.mpia-hd.mpg.de/homes/dullemon/radtrans/

Tau (discussed below) this will also be inconclusive. HST observations show that the asymmetry can change from one side to the other in no more than about six months but do not significantly constrain a lower limit on the period or, indeed, demonstrate that the variability is periodic rather than stochastic. Since the net polarization vectors of the two sides of the bright nebula are not parallel (see Fig. 6 of *Whitney and Hartmann*, 1992), the asymmetry should produce a polarimetric signature. On-going polarimetric monitoring of HH 30 may help to determine the timescale of the asymmetry.

2.4.3 AA Tau. AA Tau seems to be a prototype for both mechanisms suggested to explain the morphological variability of HH 30, apparently possessing both inclined hot spots and occulting inner-disk warps (*Bouvier et al.*, 1999; *Ménard et al.*, 2003; *O'Sulivan et al.*, 2005), both the result of an inclined stellar magnetic dipole. The disk around AA Tau has recently been imaged in scattered light by *Grady et al.* (in preparation), although previous observations with similar sensitivities did not detect the disk. It seems that the disk was finally detected because it was observed at an epoch in which the inner-disk warp was at least partially occulting the star.

2.4.4 Other Disks. It would be useful to be able to compare the variability in HH 30 to other disks, to understand what is unusual and what is common. In this respect, recent second-epoch observations of several objects by *Cotera et al*. (in preparation) are very useful. Nevertheless, since most disks have been observed at only one or two epochs, there is little that we can say about their variability.

3. MODELING TECHNIQUES

3.1. Radiation Transfer

There are several techniques for simulating scattered light images of disks and envelopes including the single scattering approximation (e.g., *Dent*, 1988; *Burrows et al.*, 1996; *D'Alessio et al.*, 1999) and direct integration of the equation of radiation transfer under the assumption of isotropic scattering (e.g., *Dullemond and Dominik*, 2004). However, by far the most common techniques are Monte Carlo simulations or integrations (e.g., *Lefèvre et al*, 1982, 1983; *Bastien and Ménard*, 1988, 1990; *Whitney and Hartmann*, 1992, 1993; *Lopez, Mékarnia, and Lefèvre*, 1995; *Burrows et al.*, 1996; *Whitney et al.*, 1997, 2003a,b, 2004; *Lucas and Roche*, 1997, 1998; *Stapelfeldt et al.*, 1999; *Wood et al.*, 1998, 1999, 2001; *Lucy*, 1999; *Wolf et al.*, 1999, 2002, 2003; *Bjorkman and Wood*, 2001, *Cotera et al.*, 2001; *Watson and Henney*, 2001; *Schneider et al.*, 2003; *Stamatellos and Whitworth*, 2003, 2005; *Watson and Stapelfeldt*, 2004). Faster computers and improved algorithms allow these simulations to be fast, incorporate anisotropic scattering, polarization, and fully three-dimensional circumstellar geometries and illuminations.

For optical and near-infrared simulations one can normally assume that scattered *starlight* dominates the images and there is no contribution from dust reprocessing. With this assumption, an image at a specific wavelength and orientation can be calculated in a few minutes on current computers. Simulations at longer wavelengths must include thermal reprocessing and calculate thermal equilibrium (e.g., *D'Alessio et al.*, 1998, 1999; *Whitney et al.*, 2003a,b).

Some groups have made their scattering and thermal equilibrium codes publicly available (see Table 2), and these tools are now being used by the community.

3.2. Density Distributions

Modelers take different approaches to the density distribution in disks. One extreme is to assume disks are vertically isothermal, the dust is well mixed with the gas, and the surface density and scale heights are power laws in the radius. Another extreme is to solve self-consistently for the temperature using thermal equilibrium, to solve for the vertical density distribution using pressure equilibrium, to solve for the surface density assuming an accretion mechanism with a constant mass-transfer rate, and to include dust settling. In between are many intermediate approaches, for example, solving for thermal equilibrium and vertical pressure equilibrium but imposing a surface density law.

The approaches are complementary. The simple power-law disks have very little physics, but have many "knobs" that can be arbitrarily adjusted to represent a wide range of disk density distributions and thereby cover the very real uncertainties in our understanding of these objects. On the other hand, the approaches that incorporate more and more physics have fewer and fewer "knobs". In one sense, they are more realistic, but only to the extent that our understanding of disk physics is correct. Unfortunately, there are real gaps in our knowledge. For example, thermal equilibrium

TABLE 3
PARAMETERS CONSTRAINED BY SCATTERED-LIGHT IMAGES

Inclination	Parameters
Edge-on	inclination, mass-opacity, forward scattering, and scale height
Intermediate	inclination, mass-opacity, forward scattering, and outer radius
Face-on	inclination, radial dependence of scale height

depends on the dust opacity, which is not well known; the details of accretion are still actively being researched, with disk viscosities uncertain by orders of magnitude; and disks may not have a constant inward mass-transfer rate.

Both approaches are useful, but is important to understand the strengths and weaknesses of each. Simple parameterized models allow one to investigate the dependence of other properties on the density distribution (e.g., *Chauvin et al.*, 2002; *Watson and Stapelfeldt*, 2004), but are limited in what they can tell us about disk physics. On the other hand, models with more physics are necessary to test and advance our understanding of disks (e.g., *D'Alessio et al.*, 1998, 1999; *Schneider et al.*, 2003; *Calvet et al.*, 2005), but our knowledge of the input physics in these models is still incomplete. For these reasons, future modeling efforts will continue to tailor their approaches to modeling the density distribution according to the specific problem being addressed.

3.3. Fitting

Determining how well scattered light images can be modeled is important for testing physical models of flared disks and collapsing envelopes. Many studies have been succesful at reproducing the overall morphology and intensity pattern of scattered light images (e.g., *Lucas and Roche*, 1997; *Whitney et al.*, 1997; *Wood et al.*, 2001). However, quantitative model fitting is more convincing and provides a better test of physical models. *Burrows et al.* (1996) and *Krist et al.* (2002) applied least-squares fitting techniques to single-scattering models of the disks of HH 30 and HK Tau B and determined their physical structure and scattering properties. More recently, *Watson and Stapelfeldt* (2004) applied least-squares fitting techniques to multiple-scattering models of the disk of HH 30 and allowed the density structure and dust scattering properties to be free parameters. Their results provide strong constraints on the circumstellar density, structure, and dust properties (see section 5.2). *Glauser et al.* (in preparation) have recently fitted models to scattered-light images, polarization images, and the SED of IRAS 04158+2805.

4. DISK STRUCTURE FROM SCATTERED LIGHT IMAGES

Interpreting scattered light images of optically-thick disks is an inverse problem. The physics that takes us from a three-dimensional distribution of emissivity and opacity to a two-dimensional distribution of surface brightness removes a great deal of information. In this section we discuss what information is lost and what can be recovered. The orientation from which a disk is viewed is a critical factor in this. For this reason, we classify disks as edge-on, intermediate-inclination, and face-on. The parameters that can be most directly constrained in each case are summarized in Table 3.

4.1. Edge-On Disks

Opaque material close to the equatorial plane of edge-on optically-thick disks occults the star; all that is seen at optical and near-infrared wavelengths are two nebulae formed by light scattered by material away from the equatorial plane. These nebulae tend to be dominated by material in the segment of the disk closest to the observer. The information present in the images can be summarized as follows:

1. The brightness ratio of the nebulae. This is largely sensitive to the inclination of the disk with respect to the observer. When a symmetrical star-disk system is observed in its equatorial plane, the nebulae should have equal brightness. As disk is tilted with respect to the observer, the nebula that is closer to the line of sight to the star dominates (see the top row of Fig. 4).

2. The minimum separation of the nebulae. The minimum separation occurs on the projected axis of an axisymmetric disk. It is largely sensitive to the total mass-opacity product of the disk. As the mass-opacity product of a disk is increased, the dark lane separating the two nebulae widens (see the second row of Fig. 4). A good example of this is the decreasing separation of the nebulae of HH 30 with increasing wavelength (e.g., Figs. 6 and 8 of *Cotera et al.*, 2001, and Fig. 2 of *Watson and Stapelfeldt*, 2004). One cannot use the width of the dark lane to constrain the mass or the absolute opacity individually without additional information. This is because the appearance of the disk at optical and near-infrared wavelengths is a scattering problem, and in the equations governing such problems the mass density and opacity per unit mass always appear as a product. On the other hand, one can use changes in the width of the lane to quantify relative changes in the opacity as a function of wavelength (see section 5.2).

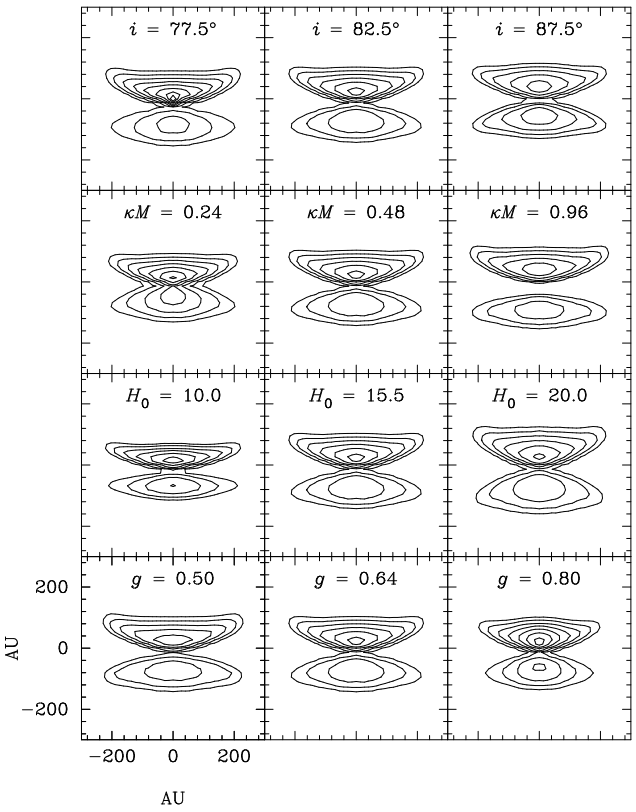

Fig. 4.— Scattered-light models of an edge-on disk. The center column shows model A1 of *Burrows et al.* (1996). The left and right columns show models with, from top to bottom, different inclinations from face-on, different mass-opacity products κM (in $\mathrm{cm}^2\,\mathrm{g}^{-1}\,\mathrm{M}_\odot$, scale height normalizations H_0 (in AU), and phase function asymmetry parameters g. The contours have the same level in each panel and are spaced by factors of 2. See *Burrows et al.* for precise definitions of the density distribution and parameters.

3. The increase in separation of the nebulae with increasing projected distance from the star. By this we refer to the degree of curvature of the boundary of the dark lane separating the two nebulae or the degree of apparent flaring of the nebulae. This is largely sensitive to the effective scale height of dust in the outer part of the disk (say, at the radii which dominate the observed scattered light). Larger scale heights lead to greater curvature or flaring (see the third row of Fig. 4). Good examples of this are the relatively flared nebulae of HH 30, which has a scale height of 16–18 AU at 100 AU, and the very flat nebulae of HK Tau B, which has a scale height of about 4 AU at 50 AU (see section 5.1).

4. The vertical extent of each individual nebula. By this we mean the apparent height of each nebula in comparison to its apparent diameter. Again, this is largely sensitive to the effective scale height of dust in the outer part of the disk. Larger scale heights lead to more extended nebulae (see the third row of Fig. 4). Good examples of this are again the vertically extended nebulae of HH 30 and the narrow nebulae of HK Tau B.

5. The degree to which the surface brightness of the nebulae drops with increasing projected distance from the star. This is largely sensitive to the degree to which forward scattering dominates the phase function. Enhanced forward scattering produces a more centrally-concentated distribution and a more pronounced decrease in surface brightness with increasing projected distance (see the fourth row of Fig. 4). The light that emerges close to the projected disk axis has scattered through relatively small angles and the light that emerges far from the projected disk axis has scattered through relatively large angles. Increased forward scattering enhances the former and diminishes the latter. A good example of this is the better fits for HH 30 obtained by *Watson and Stapelfeldt* (2004) with high values of the phase function asymmetry parameter g.

However, much information that is lost or ambiguous:

1. The luminosity of the star. All of the light we see is processed through the disk, either by scattering or by absorption and thermal emission.

2. The inner region of the disk. The observed disks appear to be sufficiently flared that the light scattered from the outer parts comes from a relatively small range of angles and passes either completely above the inner disk or through regions of the inner disk with similar extinctions. In these case, one could remove the inner 30 AU of the disk and the observed pattern of scattered light would not change, although the total brightness of scattered light might.

   An exception to this general rule may be HH 30, in which is it is possible that parts of the inner disk shadows parts of the outer disk (see section 2.4). Another exception may be disks in which the inner part of the disk shadows the outer part completely.

3. The outer radius. Scattered light images of edge-on disks sometimes show a relatively sharp outer cutoff and this is often interpreted as the outer radius of the disk. However, it is possible that the disk continues beyond the bright nebulae, but that it is shadowed. Such an extension would likely not be seen in scattered light. There is evidence that this is the case in the sihouette disk Orion 114-426, where the scattered light nebulae do not extend to the edge of the sihouette (see Fig. 2d of *McCaughrean et al.*, 1998). An extended disk like this might also be detectable in CO.

4. The radial dependence of the surface density and effective scale height. Neither of these have strong ef-

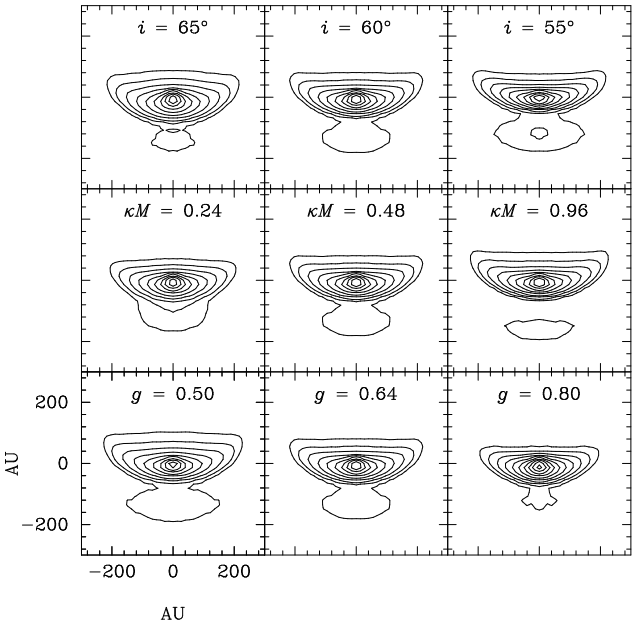

Fig. 5.— Scattered-light models of an intermediate-inclination disk. The center column shows model A1 of *Burrows et al.* (1996) inclined to 60 degrees from face-on. The left and right columns show models with, from top to bottom, different inclinations from face-on, different mass-opacity products κM (in $\mathrm{cm}^2\,\mathrm{g}^{-1}\,\mathrm{M}_\odot$, and phase function asymmetry parameters g. The contours have the same level in each panel and are spaced by factors of 2. See *Burrows et al.* for precise definitions of the density distribution and parameters.

fects on the models, at least as long as they are constrained to lie within plausible ranges. Worse, even their subtle effects are degenerate; putting more mass at larger radii produces similar effects in the images to increasing the scale height at larger radii (*Burrows et al.*, 1996; *Watson and Stapelfeldt*, 2004).

It is clear from this that scattered light images of edge-on optically-thick disks provide limited but important information on disk properties. Those which can be most cleanly separated are the inclination, the relative opacities at different wavelengths, the scale height in the outer part of the disk, and the degree of forward scattering in the phase function.

4.2. Intermediate-Inclination Disks

Intermediate-inclination disks are those in which the star is directly visible but both nebulae are still present (although one may be lost in the noise). In contrast to edge-on disks, in principle one nebulae extends over all azimuths from the star, although some azimuths may be lost in the glare of direct light from the star. Scattered-light images of intermediate-angle optically-thick disks have not been as extensively studied as edge-on disks, but preliminary studies (*Schneider et al.*, 2003; *Quijano*, 2005) suggest that the following information is present:

1. The brightness ratio of the nebulae. This depends principally on the mass-opacity product and the inclination (see the top two rows of Fig. 5).

2. The separation of the nebulae. Like the brightness ratio, this depends principally on the mass-opacity product and the inclination (see the top two rows of Fig. 5).

3. The degree to which the surface brightness drops with increasing projected distance from the star. This depends principally on the the degree to which forward scattering dominates the phase function (see the third row of Fig. 5).

4. The ratio of scattered light to unscattered light. That is, the relative brightness of the nebulae and the star. This depends on the scale height in the outer disk, the albedo, the degree to which forward scattering dominates the phase function, the inclination, and the mass-opacity product. (A complication here is that light scattered very close to the star is difficult to distinguish from direct light from the star.)

5. The outer radius. The presense of two nebulae in many systems suggests that there is not a cold, collapsed, optically-thick disk that extends significantly beyond the bright nebulae. This allows one to constrain the outer radius of the optically-thin disk with some degree of confidence. For example, GM Aur shows two nebulae which suggest that the true outer radius of the optically-thick disk is around 300 AU (*Schneider et al.*, 2003).

Again, much information is lost:

1. The inner region of the disk. In current images, information on the inner disk is lost under the PSF of the star, even when observing in polarized light (e.g., *Apai et al.*, 2004). Infrared interferometry, covered in the chapter by *Millan-Gabet et al.*, can provide a great deal of information on the very innermost part of the disk at radii of less than 1 AU. Coronagraphic images from space or, perhaps, from extreme AO systems will be required to recover information on scales larger than those available to interferometers but smaller than those lost under current PSFs.

2. The radial dependence of the surface density and effective scale height. As with edge-on disks, neither of these have strong effects on the observed morphology.

Scattered-light images of intermediate-angle optically-thick disks are thus more difficult to interpret than those of edge-on disks. The only parameter that seems to be cleanly separated is the outer radius of the disk. The mass-opacity product and the inclination are to a large degree degenerate (compare, for example, the first two rows of Fig. 5, which

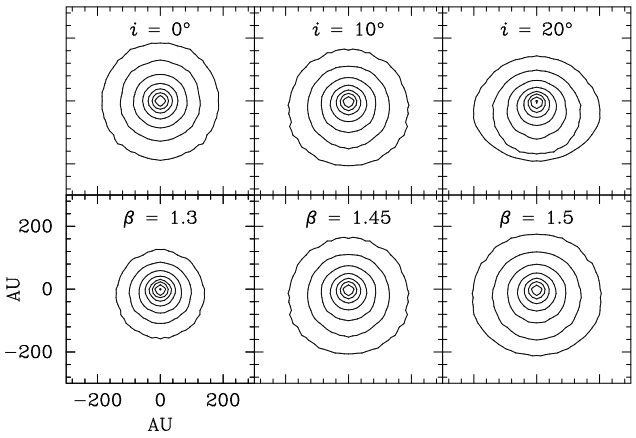

Fig. 6.— Scattered-light models of a face-on disk. The center column shows model A1 of *Burrows et al.* (1996) inclined to 10 degrees from face-on. The left and right columns show models with, from top to bottom, different inclinations from face-on and different indicies β in the scale-height power law. The contours have the same level in each panel and are spaced by factors of 2. See *Burrows et al.* for precise definitions of the density distribution and parameters.

show similar changes in the brighter nebula), but if millimeter data or an SED are available to constrain the inclination, the mass opacity product can be obtained from scattered-light images. The dust asymmetry parameter can be constrained if disk structure is known with adequate certainty.

4.3. Face-On Disks

Face-on disks are those in which departures from radial symmetry are dominated by inclination (combined with the phase function) rather than vertical structure (at least for axisymmetric star-disk systems). The only example we have of such a disk around a YSO is TW Hya (*Krist et al.*, 2000; *Trilling et al.*, 2001; *Weinberger et al.*, 2002; *Apai et al.*, 2004; *Roberge et al.*, 2005).

The information present in scattered-light images of face-on optically-thick disks is:

1. The ellipticity. This is by definition determined by the inclination and phase function in axisymmetric star-disk systems. Departures from constant ellipticity can provide a fascinating insight into non-axisymmetric illumination or disk structure. For example, *Roberge et al.* (2005) show evidence that the disk around TW Hya is significantly elliptical between 65 and 140 AU and essentially circular beyond this region; they suggest that this suggests that the disk is warped. (See the first row of Fig. 6.)

2. The dependence of the surface brightness on radius. This depends essentially on the radial dependence of the scale height. If the disk is well-mixed, this provides information on the radial dependence of the temperature. (See the second row of Fig. 6.)

3. The ratio of scattered light to unscattered light. That is, the relative brightness of the nebula and the star. This depends principally on the scale height in the outer disk, the albedo, the phase function, and the mass-opacity product.

Information on the inner disk is not present for the same reasons as in the case of intermediate-inclination disks. Information on the outer disk radius is not present for the same reasons as in the case of edge-on disks.

5. HIGHLIGHTS OF APPLIED DISK MODELING

In this section, we present four examples of scientific results from the modeling of scattered-light disks around YSOs. Our first three are related to the evolution of dust, which is also discussed in the chapters by *Natta et al.* and *Dominik et al.* The fourth concerns evidence for an inner hole in the disk around GM Aur, which may have been cleared by a planet (see the chapter by *Papaloizou et al.*). While many disks have been imaged, the cases discussed below are perhaps the best examples of how disk structure and dust properties have been derived from modeling of multi-wavelength image datasets.

5.1. Evidence for Dust Settling

The gas scale height in disks is determined by the balance between the stellar gravitational force which compresses the disk toward its midplane and gas pressure which acts to puff the disk up. In vertical hydrostatic equilibrium in a vertically isothermal disk, the gas scale height is related to the local *gas temperature* according to $H(r) = \sqrt{kT(r)r^3/GM_*m}$, where m is the mean molecular weight of the disk gas. Direct determination of the disk temperature is difficult, but reasonable results can be obtained by modeling the infrared and millimeter spectrum. A complication is that disks likely have vertical temperature inversions (*Calvet et al.*, 1991, 1992; *Chiang and Goldreich*, 1997; *D'Alessio et al.*, 1998).

If the dust and gas are well mixed, then the dust follows the gas density distribution and will have the same scale height. As we have seen in section 4.1, the dust scale height can be determined from high-resolution scattered-light images. It is important to note that the height of the scattering surface above the disk plane is not equal to the dust scale height; rather, the scattering surface defines the locus of points with optical depth unity between the star and individual disk volume elements, and can be any number of dust scale heights above the midplane. The primary observational indicators of the scale height are the vertical extent of the nebula, the degree of curvature of the nebulae, and the sharpness of the dark lane. Disks with large scale heights appear more vertically extended ("fluffy") and have curved disks whereas those with small scale heights are vertically narrow and have almost parallel nebulae. Exact value for the scale height must be determined by fitting models to the images.

TABLE 4
SCALE HEIGHTS

Object	H at 50 AU	$T_{\rm equivalent}$	Reference
HH 30	6.3 AU	51 K	*Watson and Stapelfeldt* (2004)
IRAS 04302+2247	6.1 AU	48 K	*Wolf et al.* (2003)
HV Tau C	6.5 AU	35 K	*Stapelfeldt et al.* (2003)
GM Aur	3.4 AU	18 K	*Schneider et al.* (2003)
HK Tau B	3.8 AU	8 K	*Stapelfeldt et al.* (1998)

The comparison of the scale heights for the gas and dust offer a unique opportunity to test the assumption that disks are vertically well mixed. *Burrows et al.* (1996) derived an equivalent temperature from the dust scale height for the HH 30 disk at 100 AU radius under the assumption that the disk was vertically well mixed. The result was broadly consistent with expectations from a simple thermal model, and suggested that the assumption that the disk was vertically well mixed was correct.

Since *Protostar and Planets IV* dust scale heights have been derived for several other YSO disks. In two cases, HV Tau C, and IRAS 04302+2247, initial scale height derivations implied unreasonably high equivalent temperatures and it is difficult to imagine why the dust would be more extended than the gas (*Stapelfeldt et al.*, 2003; *Wolf et al.*, 2003). These appear to be caused by the presence of circumstellar envelopes in addition to the disks, with the envelopes producing more diffuse nebulosity than expected for a pure disk. By adding an envelope to the density distribution, it was possible to remove this effect, and derive dust scale heights more consistent with simple thermal models. Scale height values for these and three other disks are shown in Table 4. The scale heights in the original references have been extrapolated to a reference radius of 50 AU to facilitate comparison.

The dust scale heights measured to date fall into two groups with the values differing by almost a factor of two. The three objects with larger scale heights all have outflows indicating ongoing accretion, whereas the two objects with smaller scale heights have little or no outflow activity. This could be observational evidence that accreting disks are systematically more puffed-up (warmer) than non-accreting disks. The small equivalent temperature implied for the HK Tau B disk merits particular attention. Unfortunately the infrared spectral energy distribution for this disk is incomplete, so this value cannot be compared to a well-constrained disk thermal model. However, it is highly unlikely that the gas in the disk could actually be as cold as 8 K. Instead, this could be a case where the assumption that the dust and gas are well mixed is not correct. Instead, it appears more likely that the dust has decoupled from the gas and partially settled toward the disk midplane, an expected stage of disk evolution (*Dubrulle et al.* 1995; *Dullemond and Dominik*, 2004). In this case, the equivalent temperature derived from the dust scale height would be lower than the true gas temperature.

The vertical scale height of dust in a YSO circumstellar disk could be a key indicator of its structure and evolutionary state. It would be very valuable to accumulate scale height measurements for larger numbers of edge-on disks, to see how unique the HK Tau B results are and uncover the full diversity of scale heights in the YSO disk population.

5.2. Evidence for Dust Growth from the Opacity Law

In optically thin media, the color of scattered light directly depends on the wavelength dependence of the grain opacity. Small grains like those in the ISM have a much higher scattering cross section at shorter wavelengths, and thus optically thin nebulae will have strongly blue colors relative to their illuminating star. However, YSO disks are optically thick in the optical and near-infrared. In this situation the color of the scattered light no longer depends on the grain opacity, and the disk will appear spectrally neutral relative to the star – even if small grains are the dominant scatterers. Neutral colors have been observed for the disks of TW Hya (*Krist et al.*, 2000; *Weinberger et al.*, 2002; *Roberge et al.*, 2005) and GM Aur (*Schneider et al.*, 2003), consistent with this expectation. A mechanism that can produce non-stellar colors in reflection from an optically thick disk is a wavelength-dependent dust albedo or phase function, but this is thought to be a small effect. Given these considerations, how can scattered light from an optically thick disk be used to constrain the grain properties?

The answer is to study changes in nebular spatial structure as a function of wavelength. For small ISM-like particles, the $\tau = 1$ scattering surface is located in lower-density regions above the disk midplane at optical wavelengths, and shifts into higher-density regions nearer the midplane at near-infrared wavelengths. Conversely, large grains acting as grey scatterers would produce a reflection nebula whose spatial structure would not vary with wavelength.

For edge-on disks, the key observable is a narrowing of the central dust lane as the object is imaged at progressively longer wavelengths (see the second row of Fig. 4). This behavior is seen in Orion 114-426 (*McCaughrean et al.*, 1998), IRAS 04302+2247 (*Padgett et al.*, 1999), HH 30 (*Cotera et al.*, 2001), and HV Tau C (*Stapelfeldt et al.*, 2003). It provides clear evidence that the scattering dust

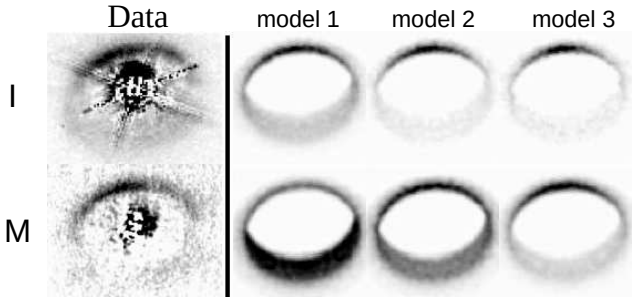

Fig. 7.— A comparison of data and models for the GG Tau circumbinary ring, in the I band (0.8 μm; top row) and M band (3.8 μm; bottom row). The ring is inclinced 37° from face on, with the forward scattering edge projected above the binary, and backscattering side projected below the binary. The key observable is the brightness contrast between the front and back sides. The first model has a maximum grain size of 0.3 μm. It matches the I band image well, but in the M band it predicts too much backscattering and not enough forward scattering. The second model has a maximum grain size of 0.9 μm. In this model, the backscattered flux becomes too small in the I band, and still too large in the M band. A reasonable mach to the M band image is obtained in the third model (maximum grain size of 1.5 μm), but the I band backscattering is underpredicted. No single grain size distribution accounts for the phase function effects at both wavelengths. Figure and results from *Duchêne et al.* (2004).

grains are dominated by small particles. But how small? A quantitative answer can be derived by fitting scattered light models to multiwavelength image data sets. This was first done in the case of HH 30 by *Cotera et al.* (2001). From modeling of HST near-infrared images, they found that the dust lane thickness changed less quickly with wavelength than expected for standard interstellar grains, and interpreted this as evidence for grain growth in the disk. *Watson and Stapelfeldt* (2004) extended this analysis by including optical images and by considering a wider range of possible density structures, but found essentially the same result: the most likely ratio of grain opacities between 0.45 and 2.0 μm is 2.0 for the HH 30 disk, versus a value of 10 expected for ISM grain models.

While the disk of HH 30 appears to show some grain evolution, modeling of multiwavelength images of the edge-on disks of HV Tau C (*Stapelfeldt et al.*, 2003) and IRAS 04302+2247 (*Wolf et al.*, 2003) finds grain opacity ratios consistent with standard ISM grains. Both of these sources possess circumstellar envelopes in addition to disks, so the presence of primitive grains could reflect this ongoing infall from the ISM onto the disks. The disk of HK Tau B shows only subtle changes in its dust lane thickness between optical and near-IR images, and may represent a more evolved system; a firm conclusion on its dust properties can be expected from future model fitting. Dust properties in the giant edge-on silhouette disk Orion 114-426 are uncertain; *Throop et al.* (2001) found the radial extent of the silhouette to be achromatic between 0.66 and 1.87 μm; *Shuping et al.* (2003) found that it was chromatic between 1.87 and 4.05 μm; while *McCaughrean et al.* (1998) showed that the dust lane thickness between the lobes of reflected light was clearly chromatic between 1.1 and 2.0 μm. Additional modeling of this source is needed. Observations and modeling of a broader sample of edge-on disks offer an opportunity to probe the diversity of dust properties across the variables of disk age, disk enviroment, and accretion signatures, and should be vigorously pursued.

5.3. Evidence for Dust Stratification from the Phase Function

GG Tau is a binary T Tauri star with 0.3″ (42 AU) projected separation. It hosts the most prominent example of a circumbinary ring of dust and gas. The ring has been studied in the millimeter lines and continuum (*Guilloteau et al.*, 1999; *Wood et al.*, 1999), near-infrared scattered light (*Roddier et al.*, 1996; *Wood et al.*, 1999; *Silber et al.*, 2000; *McCabe et al.*, 2002), and optical scattered light (*Krist et al.*, 2002, 2005). Through these studies, the density structure of the GG Tau ring is perhaps now the best understood of all YSO disks. A key feature of the ring is its intermediate inclination of 37° from face on. This spatially separates both the foreground and background parts of the ring from each other and from the central binary. This "clean" configuration allows the relative strength of forward scattering and backscattering to be directly measured. This quantity can be a powerful diagnostic of dust properties in the ring.

The scattering phase function strongly favors forward scattering when the grain size is comparable to the wavelength. At wavelengths much larger than the grain size, scattering becomes more isotropic. A comprehensive study of phase function effects in the GG Tau ring was recently carried out by *Duchêne et al.* (2004). Using new images taken at 3.8 μm, the longest wavelength to date at which scattered light from the ring has been detected, and existing images at shorter wavelengths, *Duchêne et al.* modeled the wavelength dependence of the phase function from 0.8 to 3.8μm. Highlights from their results are shown in Fig. 7. The results show that the 3.8 μm scattered light must arise from dust grains larger than those in the ISM, whereas the 0.8 μm scattered light must simultaneously originate from much smaller particles. Additional evidence for small particles is provided by the 1.0 μm polarimetry of *Silber et al.* (2000), who found the backscattered light was highly polarized and thus dominated by submicron grains.

The GG Tau phase function results indicate that no single power-law distribution of grain sizes can simultaneously account for the observations. *Duchêne et al.* (2004) suggest that these results can be explained by a vertically stratified disk in which the grain size increases towards the midplane. In this view, large grains responsible for the 3.8 μm scattered light would be located in a denser region closer to the disk midplane, a region that shorter wavelength photons cannot reach. The stratification could be due to dust settling to the ring midplane. Alternatively, it might be the case that the preference for scattering at grain sizes comparable to

the wavelength is so strong that the large grains dominate the 3.8 μm scattered light, even though they are less numerous than the small grains. In that case, vertical dust settling would not necessarily have taken place.

This picture is very attractive. However, *Krist et al.* (2005) point out that current models of GG Tau do not fully explain the observations. For example, no current model simultaneously reproduces the total brightness of the disk, its color, and its azimuthal variation. Furthermore, the ratio of brightness of the near and far parts of the disk has been observed to vary with time. Additional observations and models will be required to confirm the suggestion of a stratified disk. It would be very valuable to perform a similar study in other disk systems; unfortunately, the GG Tau ring is currently unique.

5.4. Combining Scattered Light Images and SEDs

GM Aur has a disk viewed at an intermediate inclination. The disk is clearly seen in WFPC2 and NICMOS images after careful subtraction of a reference PSF. Scattered light is detected between 0.4″ and 2.1″ (55 and 300 AU) from the star. Modeling of the scattered light images by *Schneider et al.* (2003) derived a dust vertical scale height of 8 AU at a radius of 100 AU and a disk inclination 56° from face-on, and demonstrated that there was also a remnant circumstellar envelope. However, the coronagraphic occulting spot used for the observations blocked any information on the properties of the inner disk. To access that region, *Schneider et al.* turned to the infrared spectral energy distribution (SED). Emission between 2 and 70 μm probes the disk temperature structure inside 40 AU, and thus is complementary to the results of the scattered light modeling. Using the disk model derived from the scattered light images, and appropriate assumptions about grain properties, *Schneider et al.* were able to reproduce GM Aur's SED, including the millimeter continuum points (see Fig. 8). The very small near-IR excess emission requires that the inner part of the disk be optically thin. *Rice et al.* (2003) showed that the inner region may have been cleared by a Jovian-mass planet.

More recently, *Calvet et al.* (2005) have presented *Spitzer* IRS spectroscopy of GM Aur. This data requires an inner optically-thin region that extends to 24 AU from the star. This is much larger than previous estimates based on modeling of broad-band mid-infrared photometry. The *Spitzer* IRS data show that the inner disk is not empty, but contains a small amount of small dust grains which produce the silicate emission feature. To fit the long wavelength SED, the average grain size in the outer disk must be larger than in the inner, optically-thin region.

Scattered light images do not generally provide information on the inner part of the disk. In addition to IRAS data, high-quality mid-infrared spectra from the *Spitzer Space Telescope* are becoming available for many YSO disks. Scattered light images reduce many of the degrees of freedom in modeling disk spectra and SEDs, leading directly to more robust SED models. Future combined studies of multiwavelength disk images, continuum spectra, and SEDs will provide critical tests for models of disk evolution.

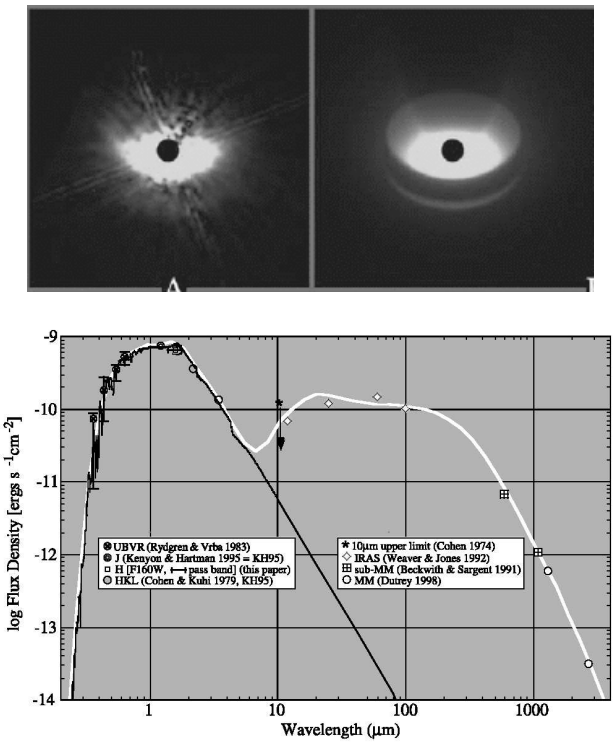

Fig. 8.— Scattered light images and SEDs of the classical T Tauri star GM Aur (*Schneider et al.*, 2003). The top left panel shows the scattered light image and the top left a model. The lower panel shows the SED. The dark line is a model for the stellar photosphere emission. The white line shows a model combining the stellar emission and the disk excess emission, with disk model parameters taken from scattered light results. For the photometry references, see *Schneider et al.* (2003).

6. PROSPECTS FOR FUTURE ADVANCES

6.1. Science Goals

The science goals for scattered-light imaging of disks around YSOs center on gaining a better understanding of disk structure, disk evolution, and dust evolution in the context of planet formation.

A key goal is to determine an evolutionary sequence for dust, especially dust growth and changes in shape and composition. One manifestation of dust evolution is to change the dust opacity law. Work in HV Tau C and HH 30 has shown that the opacity law can be determined from HST images in the optical and near-infrared using current modeling codes. Extending this work is simply a matter of obtaining the relevant observations and "cranking the handle". Observations of thermal emission at longer wavelengths will help to restrict the degeneracies in the scattered light modeling. We would expect to find disks with different opacity laws, some with near-ISM opacity laws like HV Tau C and others with less opacity laws like HH 30. The science will come from comparing the opacity laws with models for dust evo-

lution and from correlating the opacity laws with system properties such as age, accretion activity, disk mass, and stellar multiplicity.

The evidence for dust settling discussed in section 5.1 is as yet tentative. To advance, we need to be able to confidently compare the equivalent temperatures derived from the dust scale heights to the real temperatures in the disk or, more generally, the vertical distributions of the dust and the gas. This will require detailed calculations of the structure of the disk that solve for the vertical structure under the assumption of thermal equilibrium but allow for uncertainties in the radial structure. Again, including mid-infrared and millimeter data will be very useful.

Of course, we are ultimately interested in detecting young planets in disks, and especially those planets that are still accreting. Direct detection will be difficult (see the chapters by *Beuzit et al.* and *Beichman et al.*), but we can hope to observe the gap cleared by a planet as it grows. At the moment, these are most clearly seen in infrared spectra, and the contribution of scattered light images is mainly to reduce the number of degrees of freedom in the disk geometry and inclination and thereby improve the reliability of the models for the infrared emission.

We would like to understand the transition between optically-thick protoplanetary disks and optically-thin debris disks in order to determine the timescale over which planetesimals and gas – the building blocks of planet formation – are present. Advances are being made in this field with *Spitzer* imaging and spectroscopy. Scattered light imaging can contribute because small amounts of dust can potentially be detected even at radii at which infrared detections are difficult, although the realization of this goal will require advances in high-contrast imaging.

6.2. Instrument Advances

The biggest instrumental advance for the study of YSO disks will be the advent of the Atacama Large Millimeter Array (ALMA). With spatial resolution surpassing that of HST, very high resolution spectroscopy for chemical and kinematic studies, and the sensitivity to study the disks of low-mass stars as far away as Orion, ALMA will have a major impact on the field. However, even in the era of ALMA, scattered light imaging will still make significant contributions to disk studies. First, scattered light traces the surface where stellar photons deliver energy to the disk. It will still be necessary to characterize this interaction region if the disk temperature structure, and thus its chemical nature, is to be understood. Secondly, while millimeter wavelengths probe large particle sizes in the dust population, scattered light imaging provides information on the small particles. Both are needed to provide a full picture of disk grain properties and their time evolution. The combination of millimeter maps and scattered light images at comparable resolutions will be a powerful synthesis for disk science efforts.

The imaging performance of large groundbased telescopes can be expected to continue its evolution. Particularly important will be new extreme adaptive optics instruments at the Gemini and VLT observatories. Their improved contrast performance should enable additional detections of YSO disks in the near- and mid-infrared. The maturation and increasing application of differential imaging polarimetry should also yield exciting results. Several concepts for extremely large (D $\sim$ 30 m) telescopes are now being studied. When realized (maybe not until after *Protostars and Planets VI*), these facilities will provide a threefold advance in spatial resolution. Higher resolution images will improve our knowledge of all aspects of disk structure. The inner holes in systems such as TW Hya and perhaps GM Aur should be resolvable. An exciting possibility is the detection of hot young planets near to and perhaps even within YSO disks and characterization of their dynamical interactions.

Among future space missions in design and development, two will provide important capabilities for disk scattered light imaging. The NASA/ESA James Webb Space Telescope will have a 6.5 m primary mirror and operate from 1 to 28 μm. It will be a superb telescope for imaging disks in mid-infrared scattered light and will provide roughly 0.2$''$ resolution. In the near-infrared, it will offer almost three times better resolution than HST, but is unlikely to provide improved contrast. From the point of view of high contrast imaging, the Terrestrial Planet Finder Coronagraph mission would be extremely exciting, as it would be able to detect scattered light from disks as tenuous as our own solar system's zodiacal light. However, as this misssion may be more than a decade away, several groups are proposing smaller coronagraphic space telescopes that might be realized sooner.

While waiting for these future developments, the expanded application of existing scattered light imaging capabilities (AO and mid-IR imaging from large ground-based telescopes and high-contrast imaging with HST) should continue unabated.

6.3. Modeling Advances

The new observations described in this review and the observation advances outlines above suggest a wealth of detailed data on circumstellar disks will become available. What will this data demand from the codes and models?

Future codes will need to produce high-resolution images and integrated spectra at wavelengths stretching from the optical to the millimeter. They should be able to model three-dimensional distributions of sources and opacity and should incorporate accurate dust scattering phase functions, polarization, and the effects of aligned grains. Evidence for dust growth and sedimentation requires that codes no longer restrict themselves to homogenoeus dust properties, but must be able to treat multiple dust species with different spatial distributions. They will probably solve for radiation transfer using Monte Carlo techniques in optically thin regions and the diffusion approximation in optically thick regions. Computers are expected to become increasingly

parallel in the future. Many codes can already run in parallel, but those that cannot will need to be modified to do so. In this context, Monte Carlo algorithms have the advantage over classical algorithms as they often have natural parallelism. Many radiation transfer codes now have the capability to determine the density structure from given disk physics or incorporate density structures from dynamical simulations. These will be increasingly useful in providing detailed tests of disk structure. On the other hand, parameterized density models will continue to be a useful tool for mitigating our incomplete knowledge of disk physics.

The combination of future data and future codes will allow us to study dust properties, dust settling, disk structure, disk-planet interactions, accretion, and disk evolution. In the longer term, advances in techniques for numerical simulations coupled with increases in computing power and parallel processing make accurate radiation hydrodynamic simulations of disk formation and evolution a distant but realistic goal.

Perhaps the most important near-term work is to apply scattered light modeling techniques across already extant disk image datasets. Observers have provided a significant number of new, high-quality images, but the corresponding modeling efforts have not kept pace.

We thank an anonymous referee for comments that helped to improve this chapter. This work was partially supported by the Centro de Radioastronomía y Astrofísica of the Universidad Nacional Autónoma de México, HST GO program 9424 funding to the Jet Propulsion Laboratory of the California Insitute of Technology, and the Programme National de Physique Stellaire (PNPS) of CNRS/INSU, France.

REFERENCES

Apai D., Pascucci I., Brandner W., Henning Th., Lenzen R., et al. (2004) *Astron. & Astrophys., 415*, 671–676.

Ardila D. R., Lubow S. H., Golimowski D. A., Krist J. E., Clampin M., et al. (2005) *Astrophys. J., 627*, 986–1000.

Augereau J.-C. and Papaloizou J. C. B. *Astron. & Astrophys., 414*, 1153–1164.

Augereau J.-C., Lagrange A.-M., Mouillet D., and Ménard F. (1999) *Astron. & Astrophys., 350*, L51–L54.

Augereau J.-C., Lagrange A.-M., Mouillet D., and Ménard F. (2001) *Astron. & Astrophys., 365*, 78–89.

Bally J., O'Dell C. R., and McCaughrean M. J. (2000) *Astron. J., 119*, 2919–2959.

Basri G. and Batalha C. (1990) *Astrophys. J., 363*, 654–669.

Bastien P. and Ménard F. (1988) *Astrophys. J., 326*, 334–338.

Bastien P. and Ménard F. (1990) *Astrophys. J., 364*, 232–241.

Bjorkman J. E. and Wood K. (2001) *Astrophys. J., 554*, 615–623.

Bouvier J., Chelli A., Allain S., Carrasco L., Costero R., et al. (1999) *Astron. & Astrophys., 349*, 619–635.

Brandner W., Sheppard S., Zinnecker H., Close L., Iwamuro F., et al. (2000a) *Astron. & Astrophys., 364*, L13–L18.

Brandner W., Grebel E. K., Chu Y.-H., Dottori H., Brandl B., et al. (2000b) *Astron. J., 119*, 292–301.

Burrows C. J., Stapelfeldt K. R., Watson A. M., Krist J. E., et al. (1996) *Astrophys. J., 473*, 437–451.

Calvet N., Patino A., Magris G. C., and D'Alessio P. (1991) *Astrophys. J., 380*, 617–630.

Calvet N., Magris G. C., Patino A., and D'Alessio P. (1992) *Rev. Mex. Astron. Astrofis., 24*, 27–42.

Calvet N., D'Alessio P., Watson D. M., Franco–Hernández R., Furlan E., et al. (2005) *Astrophys. J., 630*, L185–L189.

Chauvin G., Ménard F., Fusco T., Lagrange A.-M., Beuzit J.-L., et al. (2002) *Astron. & Astrophys., 394*, 949–956.

Chen C. H. and Jura M. (2003) *Astrophys. J., 591*, 267–274.

Chiang E. I. and Goldreich P. (1997) *Astrophys. J., 490*, 368–376.

Clampin M., Krist J. E., Ardila D. R., Golimowski D. A., et al. (2003) *Astron. J. 126*, 385–392

Cotera A. S., Whitney B. A., Young E., Wolff M. J., Wood K., et al. (2001) *Astrophys. J., 556*, 958–969.

D'Alessio P., Cantó J., Calvet N., and Lizano S. (1998) *Astrophys. J., 500*, 411–427.

D'Alessio P., Calvet N., Hartmann L., Lizano S., and Cantó J. (1999) *Astrophys. J., 527*, 893–909.

Dent W. R. F. (1988) *Astrophys. J., 325*, 252–265.

Dubrulle B., Morfill G., and Sterzik M. (1995) *Icarus, 114*, 237–246

Duchêne G., McCabe C., Ghez A. M., and Macintosh B. A. (2004) *Astrophys. J., 606*, 969–982.

Dullemond C. P. and Dominik C. (2004) *Astron. Astrophys., 421*, 1075–1086.

Fukugawa M., Tamura M., Itoh Y., Hayashi S. S., and Oasa Y. (2003) *Astrophys. J., 590*, L49–L52.

Fukagawa M., Hayashi M., Tamura M., Itoh Y., Hayashi S. S., et al. (2004) *Astrophys. J., 605*, L53–L56.

Grady C. A., Woodgate B., Bruhweiler F. C., Boggess A., Plait P., et al. (1999) *Astrophys. J., 523*, L151–L154.

Grady C. A., Devine D., Woodgate B., Kimble R., Bruhweiler F. C., et al. (2000) *Astrophys. J., 544*, 895–902.

Grady C. A., Polomski E. F., Henning Th., Stecklum B., Woodgate B. E., et al. (2001) *Astron. J., 122*, 3396–3406.

Grady C. A., Woodgate B. E., Bowers C. W., Gull T. R., Sitko M. L., et al. (2005) *Astrophys. J., 630*, 958–975.

Grosso N., Alves J., Wood K., Neuhäuser R., Montmerle T., and Bjorkman J. E. (2003) *Astrophys. J., 586*, 296–305.

Guilloteau S., Dutrey A., and Simon M. (1999) *Astron. Astrophys., 348*, 570–578.

Hartmann L., Calvet N., Allen L., Chen H., and Jayawardhana R. (1999) *Astron. J., 118* 1748

Herbst W., Herbst D. K., Grossman E. J., and Weinstein D. (1994) *Astron. J., 108*, 1906–1923.

Hodapp K. W., Walker C. H., Reipurth B., Wood K., Bally J., et al. (2004) *Astrophys. J., 601*, L79–L82.

Jayawardhana R., Luhman K. L., D'Alessio P., and Stauffer J. R. (2002) *Astrophys. J., 571*, L51–L54

Krist J. E., Stapelfeldt K. R., Ménard F., Padgett D. L., and Burrows C. J. (2000) *Astrophys. J., 538*, 793–800.

Krist J. E., Stapelfeldt K. R., and Watson A. M. (2002) *Astrophys. J., 570*, 785–792

Krist J. E., Stapelfeldt K. R., Golimowski D. A., Ardila D. R., Clampin M., et al. (2005) *Astron. J 130*, 2778–2787.

Lefèvre J., Bergeat J., and Daniel J.-Y. (1982) *Astron. Astrophys., 114*, 341–346.

Lefèvre J., Bergeat J., and Daniel J.-Y. (1983) *Astron. Astrophys., 121*, 51–58.

Liu W. M., Hinz P. M., Meyer M. R., Mamajek E. E., Hoffmann W. F., and Hora J. L. (2003) *Astrophys. J., 598*, L111–L114

Liu W. M., Hinz P. M., Hoffmann W. F., Brusa G., Miller D., and Kenworthy M. A. (2005) *Astrophys. J., 618*, L133–L136
Lopez B., Mékarnia D., and Lefèvre J. (1995) *Astron. Astrophys., 296*, 752–760.
Lucas P. W. and Roche P. F. (1997) *Mon. Not. R. Astr. Soc., 286*, 895–919.
Lucas P. W. and Roche P. F. (1998) *Mon. Not. R. Astr. Soc., 299*, 699–722.
Lucy L. B. (1999) *Astron. Astrophys., 344*, 282–288.
McCabe C., Duchene G., and Ghez A. M. (2002) *Astrophys. J., 575*, 974–988.
McCabe C., Duchêne G., and Ghez A. M. (2003) *Astrophys. J., 588*, L113–L116.
McCaughrean M. J., Stapelfeldt K. R., and Close L. M. (2000) In *Protostars and Planets IV* (V. Mannings et al., eds.) pp. 485–507. Univ. of Arizona Tucson.
McCaughrean M. J., Chen H., Bally J., Erickson E., Thompson R., et al. (1998) *Astrophys. J., 492*, L157–L161.
Ménard F., Bouvier J., Dougados C., Mel'nikov S. Y., and Grankin K. N. (2003) *Astron. Astrophys., 409*, 163–167.
Monin J.-L., and Bouvier J. (2000) *Astron. Astrophys., 356*, L75–L78.
Mouillet D., Lagrange A. M., Augereau J.-C., and Ménard F. (2001) *Astron. Astrophys., 372*, L61–L64.
O'Sullivan M., Truss M., Walker C., Wood K., Matthews O., et al. (2005) *Mon. Not. R. Astron. Soc., 358*, 632–640.
Padgett D. L., Brandner W., Stapelfeldt K. R., Strom S. E., Terebey S., and Koerner D. (1999) *Astron. J., 117*, 1490–1504.
Pantin E., Waelkens C., and Lagage P. O. (2000) *Astron. Astrophys., 361*, L9–L12.
Pantin E., Bouwman J., and Lagage P. O. (2005) *Astron. Astrophys., 437*, 525–530.
Perrin M. D., Graham J. R., Kalas P., Lloyd J. P., Max C. E., et al. (2004) *Science 303*, 1345–1348.
Pontoppidan K. M., Dullemond C. P., van Dishoeck E. F., Blake G. A., Boogert A. C. A., et al. (2005) *Astrophys. J., 622*, 463–481.
Potter D. E., Close L. M., Roddier F., Rodder C., Graves J. E., and Northcott M. (2000) *Astrophys. J., 540*, 422–428.
Potter D. E. (2003) Ph. D. thesis (University of Hawaii).
Quijano B. (2005) Undergraduate Thesis (Universidad Michoacana de San Nicolas de Hidalgo, Morelia, Mexico).
Quillen A. C., Varnière P., Minchev I., and Frank A. (2005) *Astron. J., 129*, 2481–2495.
Rice W. K. M., Wood K., Armitage P. J., Whitney B. A., and Bjorkman J. E. (2003), *Mon. Not. R. Astron. Soc., 342*, 79–85.
Roberge A., Weinberger A. J., and Malmuth E. M. (2005) *Astrophys. J., 622*, 1171–1181.
Roddier C., Roddier F., Northcott M. J., Graves J. E., and Jim K. (1996) *Astrophys. J., 463*, 326–335.
Schneider G., Wood K., Silverstone M. D., Hines D. C., Koerner D. W., et al. (2003) *Astron. J., 125*, 1467–1479.
Shuping R. Y., Bally J., Morris M., and Throop H. (2003) *Astrophys. J., 587*, L109–L112.
Silber J., Gledhill T., Duchêne G., and Ménard F. (2000) Ap. J. 536 L89–L92.
Simon M., Dutrey A., and Guilloteau S. (2000) *Astrophys. J., 545*, 1034–1043.
Stecklum B., Launhardt R., Fischer O., Henden A., Leinert Ch., and Meusinger H. (2004) *Astrophys. J., 617*, 418–424.
Stecklum B., Henning T., Feldt M., Hayward T. L., Hoare M. G., et al. (1998) *Astron. J., 115*, 767–776.
Smith N., Bally J., Licht D., and Walawender J. (2005) *Astron. J., 129*, 382–392
Stamatellos D. and Whitworth A. P. (2003) *Astron. Astrophys., 407*, 941–955
Stamatellos D. and Whitworth A. P. (2005) *Astron. Astrophys., 439*, 153–158
Stapelfeldt K. R., Krist J. E., Ménard F., Bouvier J., Padgett D. L., and Burrows C. J. (1998) *Astrophys. J., 502*, L65–L69.
Stapelfeldt K. R., Watson A. M., Krist J. E., Burrows C. J., Crisp D., et al. (1999) *Astrophys. J., 516*, L95–L98.
Stapelfeldt K. R., Ménard F., Watson A. M., Krist J. E., Dougados C., et al. (2003) *Astrophys. J., 589*, 410–418.
Throop H. B., Bally J., Esposito L. W., and McCaughrean M. (2001) *Science 292*, 1686–1689.
Trilling D. E., Koerner D. W., Barnes J. W., Ftaclas C., and Brown R. H. (2001) *Astrophys. J., 552*, L151–L154.
Watson A. M. and Henney W. J. (2001) *R. Mex. Ast. Astrof., 37*, 221–236.
Watson A. M. and Stapelfeldt K. R. (2004) *Astrophys. J., 602*, 860–874.
Weinberger A. J., Becklin E. E., Schneider G., Smith B. A., Lowrance P. J., et al. (1999) *Astrophys. J., 525*, L53–L56.
Weinberger A. J., Becklin E. E., Schneider G., Chiang E. I., Lowrance P. J., et al. (2002) *Astrophys. J., 566*, 409–418.
White R. J. and Hillenbrand L. A. (2004) *Astrophys. J., 616*, 998–1032.
Whitney B. A. and Hartmann L. (1992) *Astrophys. J., 395*, 529–539.
Whitney B. A. and Hartmann L. (1993) *Astrophys. J., 402*, 605–622.
Whitney B. A., Kenyon S. J., and Gomez M. (1997) *Astrophys. J., 485*, 703–734.
Whitney B. A., Wood K., Bjorkman J. E., and Wolff M. J. (2003a) *Astrophys. J., 591*, 1049–1063.
Whitney B. A., Wood K., Bjorkman J. E., and Cohen M. (2003b) *Astrophys. J., 598*, 1079–1099.
Whitney B. A., Indebetouw R., Bjorkman J. E., and Wood K. (2004) *Astrophys. J., 617*, 1177–1190.
Wood K. and Whitney B. (1998) *Astrophys. J., 506*, L43–L45
Wood K., Kenyon S. J., Whitney B. A., and Turnbull M. (1998) *Astrophys. J., 497*, 404–418.
Wood K., Crosas M., and Ghez A. M. (1999) *Astrophys. J., 516*, 335–341.
Wood K., Wolk S. J., Stanek K. Z., Leussis G., Stassun K., et al. (2000) *Astrophys. J., 542*, L21–L24.
Wood K., Smith D., Whitney B. A., Stassun K., Kenyon S. J., et al. (2001) *Astrophys. J., 561*, 299–307.
Wood K., Wolff M. J., Bjorkman J. E., and Whitney B. (2002) *Astrophys. J., 564*, 887–895.
Wolf S., Henning Th., and Stecklum B. (1999) *Astron. Astrophys., 349*, 839–850.
Wolf S., Voshchinnikov N. V., and Henning Th. (2002) *Astron. Astrophys., 385*, 365–376.
Wolf S., Padgett D. L., and Stapelfeldt K. R. (2003) *Astrophys. J., 588*, 373–386.

This 2-column preprint was prepared with the AAS LaTeX macros v5.2.